

# A comparative review of recent results on supercritical anomalies in two-dimensional kinetic Ising and Blume-Capel ferromagnets

Gloria M. Buendía<sup>1\*</sup>, Celeste Mendes<sup>1,2</sup> and Per Arne Rikvold<sup>3,4\*</sup>

<sup>1</sup>Department of Physics, Universidad Simón Bolívar, Caracas, 1080, Venezuela.

<sup>2</sup>Faculdade de Ciências, Universidade do Porto, Rua do Campo Alegre, Porto, 4169-007, Portugal.

<sup>3</sup>PoreLab, NJORD Centre, Department of Physics, University of Oslo, P.O. Box 1048 Blindern, Oslo, 0316, Norway.

<sup>4</sup>Department of Physics, Florida State University, Tallahassee, Florida, 32306-4350, USA.

\*Corresponding author(s). E-mail(s): [buendia@usb.ve](mailto:buendia@usb.ve);

[p.a.rikvold@fys.uio.no](mailto:p.a.rikvold@fys.uio.no);

Contributing authors: [up202408487@edu.fc.up.pt](mailto:up202408487@edu.fc.up.pt);

## Abstract

Following the unexpected experimental discovery of “sideband” peaks in the fluctuation spectrum of thin Co films driven by a slowly oscillating magnetic field with a constant bias [P. Riego et al., Phys. Rev. Lett. **118**, 117202 (2017)] numerical studies of two-state Ising and three-state Blume-Capel (BC) ferromagnets in this dynamically supercritical regime have flourished and been successful in explaining this phenomenon. Here, we give a comparative review of this new literature and its connections to earlier work. Following an introduction and a presentation of the two models and the computational method used in many of these studies, we present numerical results for both models. Particular attention is paid to the fact that zero spins in the BC model tend to collect at the interfaces between regions of the two nonzero spin values,  $\pm 1$ . We present strong arguments that this phenomenon leads to a reduction of the effective interface tension in the BC model, compared to the Ising model.

**Keywords:** Supercritical anomalies, Kinetic Ising models, Kinetic Blume-Capel models

## 1 Introduction

Since the 1990's it has become clear that the well-known, equilibrium phase transition in the Ising universality class (e.g., a two-dimensional Ising ferromagnet in zero field at a critical temperature  $T_c$ ) has a *nonequilibrium* analog. This dynamic phase transition, commonly known as DPT, occurs when a discrete spin system in its ordered phase (i.e., below  $T_c$ ) is perturbed by an oscillating magnetic field of period  $P$ . In this case,  $P$  takes the role of  $T$  in the equilibrium case, with a critical  $P_c$  that depends on  $T$  and the field amplitude  $H_0$ . For  $P < P_c$ , the magnetization oscillates near the *equilibrium* magnetization, while for  $P > P_c$ , the system follows the sign of the field, giving a constant, period-averaged magnetization,  $\langle Q \rangle \approx 0$ .

Early studies were computational [1–4]. Kinetic Monte Carlo (MC) combined with finite-size scaling analysis [5–10], as well as mean-field studies of Ising and Ginzburg-Landau models [11–14], confirmed that this is a true DPT in the same universality class as the corresponding equilibrium Ising model. Experimental confirmations of Ising-like behavior in  $[\text{Co}/\text{Pt}]_3$  magnetic multilayers [15] and uniaxial Co films [16] were later obtained.

The close analogy in the critical region between the equilibrium Ising transition and the DPT possibly delayed studies of the DPT in the *supercritical region*,  $P > P_c$ , by several years, and the experimental results presented in 2017 by Riego, Vavassori, and Berger [17] came as a surprise. In that work, Co films with (1010) crystallographic surface structure with a single, in-plane magnetic easy axis were subjected to an oscillating magnetic field plus a constant bias field,  $H_b$ . Such a constant bias field had previously been shown to be a significant component of the field conjugate to  $\langle Q \rangle$  in the critical region near  $P_c$  [8, 12–14, 16]. In general, it favors spin transitions in the direction toward the state in which they have the same sign as  $H_b$ . However, in stark contrast to the wide, unimodal maximum of the supercritical susceptibility of the equilibrium Ising model, two distinct peaks in the corresponding response function were found at nonzero values of  $H_b$ , symmetrical about zero. These new results have inspired recent studies of DPT transitions also in the presence of nonantisymmetric and random fields and interactions [18–20].

In this short paper, we review central results from recent, kinetic MC studies of the 2D Ising ferromagnet [21] and BC model [22], both in the dynamically supercritical regime,  $P > P_c$ . The defining Hamiltonians and the MC simulation method used are presented in Sec. 2, while numerical results for the Ising model and the BC model are presented in Sec. 3 and Sec. 4, respectively. Some nucleation-theoretical results relevant for both models are discussed in Sec. 5. Conclusions and a discussion are given in Sec. 6.

## 2 Models and simulation method

We consider kinetic spin models with a time-dependent external field  $H(t)$  plus a constant “bias field”  $H_b$ , ferromagnetic nearest-neighbor interactions,  $J > 0$ , and a

crystal field,  $D$ . The defining Hamiltonian is

$$\mathcal{H} = -J \sum_{\langle ij \rangle} s_i s_j - D \sum_i s_i^2 - [H(t) + H_b] \sum_i s_i , \quad (1)$$

where the first sum runs over all nearest-neighbor pairs, and the other two over all sites.  $H(t)$  is a symmetrically oscillating external field of period  $P$ ,

$$H(t) = H_0 \cos\left(\frac{2\pi}{P}t\right) . \quad (2)$$

$H_0$ ,  $H_b$ ,  $D$  are all given in units of  $J$  (i.e.,  $J = k_B = 1$ ), where  $k_B$  is Boltzmann's constant. The systems are simulated on a square lattice of  $N = L \times L$  sites with periodic boundary conditions at constant temperature,  $T = 0.8T_c$ . If  $s_i = \pm 1$ , the  $D$  term becomes an unimportant constant, and the above Hamiltonian describes the standard Ising model. However, with  $s_i \in [\pm 1, 0]$  and  $D \in [-\infty, +\infty]$  it describes the BC model. (In the limit  $D = +\infty$ ,  $s_i = 0$  becomes forbidden, and the BC model degenerates to the two-state Ising model.) Kinetic MC simulations were performed with a time unit of one MC step per site (MCSS), during which each site was visited once on average.  $P$  is in units of MCSS. Transition probabilities were given by a heat-bath single-spin transition dynamics. A spin  $s_i$  was selected at random and changed to  $s'_i$  with probability

$$W(s_i \rightarrow s'_i) = \frac{\exp[-\beta \Delta E(s_i, s'_i)]}{\sum_{s'_i} \exp[-\beta \Delta E(s_i, s'_i)]} , \quad (3)$$

where  $\Delta E(s_i, s'_i)$  is the change in the system energy associated with changing the spin  $i$  from  $s_i$  to  $s'_i$ , and  $\beta = 1/k_B T$ .  $s_i$  and  $s'_i$  are restricted to the allowed values for each model:  $\pm 1$  for Ising and  $[\pm 1, 0]$  for BC.

Quantities calculated were the time dependent, normalized magnetization per site,

$$m(t) = \frac{1}{L^2} \sum_i s_i(t) \quad (4)$$

and its integrals over each field cycle  $k$ ,

$$Q_k = \frac{1}{P} \int_{(k-1)P}^{kP} m(t) dt . \quad (5)$$

The dynamic order parameter is the period-averaged magnetization,  $\langle Q \rangle$ , defined as the average of  $Q_k$  over many periods. Its fluctuations are measured by the scaled variance,

$$\chi_L^Q = L^2(\langle Q^2 \rangle - \langle Q \rangle^2) . \quad (6)$$

Most measurements were taken over 800 field periods, after discarding 200 periods. Thus, at least  $800 \times P$  MCSS in the supercritical region with  $P > P_c$  were performed for each measurement.

### 3 Kinetic Ising model

We first present results for the standard Ising model [21], Eq. (1) with  $s_i = \pm 1$ . Most calculations were performed with  $H_0 = 0.3$  at  $T = 0.8T_c$ , where  $T_c = 2/\ln(1 + \sqrt{2}) \approx 2.269$  is the critical temperature of the standard, square-lattice Ising model in zero field. The critical period of this oscillating field with zero bias is  $P_c \approx 258$  [6].

In Fig. 1 we present results for  $P \approx 3.9P_c$  and for several lattice sizes. Figure 1(a) shows  $\langle Q \rangle$  vs  $H_b$ . For weak  $H_b$ ,  $\langle Q \rangle$  increases almost linearly until, at  $|H_b| \approx 0.09$ , the slope increases and finally saturates for  $|H_b| \gtrsim 0.15$ . This behavior is reflected in the scaled variance  $\chi_L^Q$  shown in Fig. 1(b), which presents two symmetrical peaks located at  $|H_b| = |H_b^{\text{peak}}| \approx 0.09$ , separated by a flat-bottomed valley and saturating for strong bias. For these values of  $L$  and  $P$  we cannot see any finite-size effects that could suggest that this is a critical behavior associated with a phase transition. The appearance of these “sidebands” is consistent with the experimental results presented in Ref. [17] and clearly demonstrates that they are not due to any residual magnetostatic long-range interactions.

To explore the nature of the “sidebands” and their dependence on the system size and bias, in Fig. 2 we present short time series of the normalized magnetization,  $m(t)$ . Since  $H_b > 0$ , the up-spin phase is favored, while the down-spin phase is disfavored. Figure 2(a) was obtained on the strong-bias side. Size effects are notable in this case. For  $L = 32$  and  $64$  the switching from the favored to the disfavored magnetization is stochastic and abrupt. For the larger systems, the switching becomes more deterministic and gradual, but the spins do not have time to reach the complete down phase before the field switches to positive values. Figure 2(b) was obtained at  $H_b \approx H_b^{\text{peak}}$ . While the switching remains stochastic for  $L = 32$ , the larger systems have a more deterministic behavior and reach larger negative magnetizations than in the previous case. Figure 2(c) was obtained at  $H_b$  on the weak-bias side. The switching for  $L = 32$  remains stochastic, but all the other sizes have a deterministic behavior and perform a more complete switching toward the negative phase.

To further illustrate the different decay mechanisms in Fig. 2(b), in Fig. 3(a) we present time series for  $m(t)$  over several periods with  $P = 1000$  and a bias corresponding to the peak  $H_b^{\text{peak}} = +0.0915$ , with  $L = 32$  and  $1024$ . Snapshots taken at  $m(t) = +0.1$  (indicated by circles in the figure), when the total applied field is negative, show the nucleation and growth of droplets of the stable, disfavored spin-down phase. Figure 3(b), for  $L = 32$ , is a snapshot showing the growth of a single droplet of the stable down phase (SD regime), while Fig. 3(c) shows that for  $L = 1024$  the decay occurs by the independent nucleation, growth, and eventual coalescence of many droplets of the stable phase. This multi-droplet (MD) decay leads to a deterministic regime that is well described by the Kolmogorov-Johnson-Mehl-Avrami (KJMA) approximation [23–30].

These results clearly indicate that the “sidebands” are a result of a change of the switching mechanism. In the vicinity of the peaks, a cross-over from a stochastic single-droplet mechanism (for the smaller systems or strong bias) to a nearly deterministic multidroplet mechanism (for the larger system or weak bias), in agreement with known

**Table 1** Critical periods  $P_c$ , peak positions  $|H_b^{\text{peak}}|$ , and critical temperatures  $T_c$ , for the kinetic BC model subjected to a sinusoidal field of amplitude  $H_0 = 0.2$  for different values of crystal field  $D$  at  $T = 0.8T_c$ . The data for  $T_c$  were obtained from [44], and  $P_c$  and  $|H_b^{\text{peak}}|$  from [22] under CC-BY 4.0 license.

$D$	$P_c$ (MCSS)	$ H_b^{\text{peak}} $	$T_c$
0	$870 \pm 10$	$0.060 \pm 0.001$	$1.693(3)$
-0.5	$720 \pm 10$	$0.061 \pm 0.002$	$1.564(3)$
-1.0	$460 \pm 10$	$0.062 \pm 0.002$	$1.398(2)$
-1.5	$205 \pm 5$	$0.063 \pm 0.002$	$1.151(1)$
-1.75	$115 \pm 5$	$0.067 \pm 0.002$	$0.958(1)$

results for field-driven magnetization switching by homogeneous nucleation and growth of droplets of the stable phase [23].

## 4 Kinetic Blume-Capel model

In this section we present results for the ferromagnetic kinetic BC model [22], defined by Eq. (1) with  $s_i \in [\pm 1, 0]$ , and  $D \in [-1, +1]$ . This system has a more complex equilibrium phase diagram than the Ising model [31–35]. For high temperatures, zero magnetic field, and greater values of  $D$ , it undergoes a continuous (second-order) equilibrium transition between a ferromagnetic and a paramagnetic phase, while for low temperatures and sufficiently negative values of  $D$ , the transition is discontinuous (first-order) [36–41]. The two transition lines join smoothly at a tricritical point  $(D_t, T_t)$ . [42]. (See Fig. 1 of Ref. [22].)

For values of  $D$  and  $T < T_c$ , corresponding to the continuous equilibrium transition, the BC model in an oscillating magnetic field of period  $P$  has a DPT at a critical period  $P_c$ , analogous to the standard Ising model discussed in Sec. 3 above. This dynamic transition also belongs to the same universality class as the equilibrium Ising model [43]. In this section we show that the BC model also presents “metamagnetic” anomalies in the supercritical region,  $T < T_c$ ,  $P > P_c$ , just like the Ising model.

Heat-bath MC simulations as defined in Eq. (3) were again performed on a square lattice of linear dimension  $L$  with periodic boundary conditions, at  $T = 0.8T_c$  and with  $H_0 = 0.2$ . (Note that  $H_0$  is different from the value used in the simulations of the standard Ising model above.) For the BC model,  $T_c$  depends on  $D$ , and  $P_c$  depends on both  $D$  and  $H_0$ . In Table 1 we report the critical temperatures calculated by Malakis et al. [44] and the critical periods calculated by Mendes et al. [22] for  $H_0 = 0.2$ . The data were obtained for values of  $D$  within the region where the phase transition is continuous, and in the supercritical region where  $P(D) > P_c(D)$ , a region where, as with the Ising model, we expect to find the metamagnetic anomalies. Indeed, data for  $\langle Q \rangle$  and  $\chi_L^Q$  for different  $L$  are only weakly size dependent, qualitatively similar to those for the Ising model. Detailed results are found in Ref. [22].

As the crystal field  $D$  approaches its tricritical value from the positive side, the density of zeros increases. Figure 4 shows the results. The order parameter in Fig. 4(a)

exhibits a strong dependence on  $D$  only near  $|H_b^{\text{peak}}|$ . The slope of  $\langle Q \rangle$  around  $|H_b^{\text{peak}}|$  decreases as  $|D - D_t|$  is decreased. This is reflected in the decreasing heights of the scaled variance peak in Fig. 4(b). The results also suggest that  $|H_b^{\text{peak}}|$  increases as  $D$  closely approaches  $D_t$ . This is shown in Table 1. These results indicate that, as the density of zeros increases, stronger bias fields are needed to generate the asymmetry responsible for the sidebands, and even for these larger values of  $H_b$ , the heights of the fluctuation peaks are reduced. This is consistent with the assertion by Schick and Shih [45], that the effective interface tension should decrease in proportion to  $|D - D_t|$  close to the tricritical point.

From a very detailed study of the dependence of the sidebands on the period  $P$ , the crystal field  $D$ , and the amplitude of the oscillating field  $H_0$ , it was concluded that their behavior is analogous to that of the Ising model [22]. In the BC model, as the density of zeros is increased by letting  $D$  approach  $D_t$ , larger bias fields are needed to generate the asymmetry responsible for the sidebands. This results in flatter peaks [22].

As with the Ising model, we compare the magnetization time series for different system sizes. Stochastic behavior for  $L = 32$  and nearly deterministic behavior for  $L = 1024$  are shown in Fig. 5(a).

In Fig. 5(b) and (c) we present snapshots of the system at a point where it is in the process of going from the metastable phase to the stable one. It is clear that for the small system, Fig. 5(b), this process occurs by the growth of a single droplet of the stable phase (SD), while for the larger system, Fig. 5(c), the decay to the stable phase occurs by the independent nucleation and growth of many droplets (MD). This behavior, as in the Ising model, is consistent with nucleation theory.

From Fig. 5(b) and (c) we also notice that, in both regimes, SD and MD, the zero spins are mostly located at the interfaces between the two nonzero phases. This may result in a reduced interface tension for the BC model, compared to the Ising model [45].

## 5 Nucleation theory for the kinetic spin models

By studying the dependence of  $|H_b|$  on the period length of the external oscillating field and employing nucleation theory on the kinetic models subjected to a sinusoidal field plus a constant bias and, the following relation was expected to apply for very large periods [21, 22]

$$P \sim L^{-a} \exp \left( \frac{1}{b} \frac{\Xi_0}{H_0 - |H_b^{\text{peak}}|} \right), \quad (7)$$

with  $a = 2$  and  $b = 1$  for SD switching, and  $a = 0$  and  $b = 3$  for MD switching, where  $\Xi_0$  is the field-independent part of the free energy cost of a critical droplet divided by  $k_B T$ . For details see [21] and references therein. From this expression we expect that, if we plot  $\frac{1}{(H_0 - |H_b^{\text{peak}}|)}$  vs  $\log P$ , we will get a straight line for large  $P$ , such that the ratio between the slopes for the MD (large system) and SD (small system) regime for the same model is 3. Such plots for both the Ising and BC models are shown together in Fig. 6(a). For the Ising model, the ratio of the slopes is approximately

2.866(1) [21], and for the BC model the ratio is approximately 2.405(1) [22]. Both values, particularly the one for the Ising model, are close to the expected value of 3. A work based on effective field theory on the kinetic BC model in the presence of a bias reported a slope of 2.236 [46].

The results for the two models that are shown in Fig. 6(a) were obtained from simulations with different values of  $H_0$ , which leads to different values for  $P_c$ . In order to directly compare the results, in Fig. 6(b) we present them in terms of dimensionless variables,  $1/(1 - H_b^{\text{peak}}/H_0)$  vs  $P/P_c$ . With this scaling, the curves collapse for  $P/P_c < 10$ . For  $P/P_c > 10$ , the difference between the two models due to the zeros in the BC case is evident. In each case the behavior is consistent with the predictions of nucleation theory. From this, we can also obtain a rough estimate for the ratios of  $\Xi_0$  (which is proportional to the square of the effective interface tensions [47]) for the same system size for the two models. For  $L = 256$  we obtain  $\Xi_0(\text{BC})/\Xi_0(\text{Is}) \approx 0.658(1)$  and for  $L = 32$  we get  $\approx 0.784(1)$ . The fact that both ratios are less than unity strengthens the case that the zero state in the BC model acts as a surfactant to reduce the effective interface tension between the two nonzero phases [45, 48, 49]. A very recent study indicates that the surface-tension scaling of the BC model on a triangular lattice agrees with what has previously been observed for the square-lattice [50].

## 6 Conclusions

The experimental discovery of “sideband” peaks in the fluctuation spectrum of thin Co films driven by a slowly oscillating magnetic field with a constant bias [17] was quickly followed by a number numerical studies (see the list of references) that provided successful explanations of this nonequilibrium phenomenon. In the comparative study presented here, we show that the supercritical anomalies in the two-state Ising and the three-state BC model share many common features. These include a gradual crossover between SD switching behavior for smaller systems and MD switching for larger systems. In the MD regime, finite-size effects on the dynamic order parameter  $\langle Q \rangle$  and its fluctuations become essentially negligible. This indicates that the observed fluctuation peaks are not caused by a critical phenomenon. Rather, they are a stochastic-resonance phenomenon due to the asymmetry introduced by the bias field.

The main difference between the behaviors of the two models is that the zero spins in the BC model tend to accumulate at the interfaces between regions of positive and negative spins. This appears to lead to a reduction of the interface tension between regions of positive and negative spins in the BC model, compared with the Ising model.

Future studies may reveal further, novel effects as the dynamics of spin systems with multiple states are extended to antiferromagnetic interactions, more complicated lattices, and higher spatial dimensions.

## Acknowledgments

G.M.B. expresses her appreciation for support and hospitality at the PoreLab and NJORD Centres of the Department of Physics at the University of Oslo.

Work at the University of Oslo was supported by the Research Council of Norway through the Center of Excellence funding scheme, Project No. 262644.

## References

- [1] T. Tomé, M.J.D. Oliveira, Dynamic phase transition in the kinetic Ising model under a time-dependent oscillating field. *Phys. Rev. A* **41**, 4251 (1990). <https://doi.org/10.1103/PhysRevA.41.4251>. URL <https://journals.aps.org/pra/abstract/10.1103/PhysRevA.41.4251>
- [2] W.S. Lo, R.A. Pelcovits, Ising model in a time-dependent magnetic field. *Phys. Rev. A* **42**, 7471 (1990). <https://doi.org/10.1103/PhysRevA.42.7471>. URL <https://journals.aps.org/pra/abstract/10.1103/PhysRevA.42.7471>
- [3] M. Rao, H.R. Krishnamurthy, R. Pandit, Magnetic hysteresis in two model spin systems. *Phys. Rev. B* **42**, 856 (1990). <https://doi.org/10.1103/PhysRevB.42.856>. URL <https://journals.aps.org/prb/abstract/10.1103/PhysRevB.42.856>
- [4] B.K. Chakrabarti, M. Acharyya, Dynamic transitions and hysteresis. *Rev. Mod. Phys.* **71**, 847 (1999). <https://doi.org/10.1103/RevModPhys.71.847>. URL <https://journals.aps.org/rmp/abstract/10.1103/RevModPhys.71.847>
- [5] S.W. Sides, P.A. Rikvold, M.A. Novotny, Kinetic Ising model in an oscillating field: Finite-size scaling at the dynamic phase transition. *Phys. Rev. Lett.* **81**, 834 (1998). <https://doi.org/10.1103/PhysRevLett.81.834>. URL <https://journals.aps.org/prl/abstract/10.1103/PhysRevLett.81.834>
- [6] S.W. Sides, P.A. Rikvold, M.A. Novotny, Kinetic Ising model in an oscillating field: Avrami theory for the hysteretic response and finite-size scaling for the dynamic phase transition. *Phys. Rev. E* **59**, 2710 (1999). <https://doi.org/10.1103/PhysRevE.59.2710>. URL <https://journals.aps.org/pre/abstract/10.1103/PhysRevE.59.2710>
- [7] G. Korniss, C.J. White, P.A. Rikvold, M.A. Novotny, Dynamic phase transition, universality, and finite-size scaling in the two-dimensional kinetic Ising model in an oscillating field. *Phys. Rev. E* **63**, 016120 (2000). <https://doi.org/10.1103/PhysRevE.63.016120>. URL <https://journals.aps.org/pre/abstract/10.1103/PhysRevE.63.016120>
- [8] D.T. Robb, P.A. Rikvold, A. Berger, M.A. Novotny, Conjugate field and fluctuation-dissipation relation for the dynamic phase transition in the two-dimensional kinetic Ising model. *Phys. Rev. E* **76**, 021124 (2007). <https://doi.org/10.1103/PHYSREVE.76.021124/FIGURES/12/MEDIUM>. URL <https://journals.aps.org/pre/abstract/10.1103/PhysRevE.76.021124>
- [9] G.M. Buendía, P.A. Rikvold, Dynamic phase transition in the two-dimensional kinetic Ising model in an oscillating field: Universality with respect to the

stochastic dynamics. *Phys. Rev. E* **78**, 051108 (2008). <https://doi.org/10.1103/PHYSREVE.78.051108/FIGURES/7/MEDIUM>. URL <https://journals.aps.org/pre/abstract/10.1103/PhysRevE.78.051108>

[10] H. Park, M. Pleimling, Dynamic phase transition in the three-dimensional kinetic Ising model in an oscillating field. *Phys. Rev. E* **87**, 032145 (2013). <https://doi.org/10.1103/PHYSREVE.87.032145/FIGURES/4/MEDIUM>. URL <https://journals.aps.org/pre/abstract/10.1103/PhysRevE.87.032145>

[11] H. Fujisaka, H. Tutu, P.A. Rikvold, Dynamic phase transition in a time-dependent Ginzburg-Landau model in an oscillating field. *Phys. Rev. E* **63**, 036109 (2001). <https://doi.org/10.1103/PhysRevE.63.036109>. URL <https://journals.aps.org/pre/abstract/10.1103/PhysRevE.63.036109>

[12] R.A. Gallardo, O. Idigoras, P. Landeros, A. Berger, Analytical derivation of critical exponents of the dynamic phase transition in the mean-field approximation. *Phys. Rev. E* **86**, 051101 (2012). <https://doi.org/10.1103/PHYSREVE.86.051101/FIGURES/5/MEDIUM>. URL <https://journals.aps.org/pre/abstract/10.1103/PhysRevE.86.051101>

[13] O. Idigoras, P. Vavassori, A. Berger, Mean field theory of dynamic phase transitions in ferromagnets. *Phys. B (Amsterdam, Neth.)* **407**, 1377–1380 (2012). <https://doi.org/10.1016/J.PHYSB.2011.06.029>

[14] D.T. Robb, A. Ostrander, Extended order parameter and conjugate field for the dynamic phase transition in a Ginzburg-Landau mean-field model in an oscillating field. *Phys. Rev. E* **89**, 022114 (2014). <https://doi.org/10.1103/PHYSREVE.89.022114/FIGURES/6/MEDIUM>. URL <https://journals.aps.org/pre/abstract/10.1103/PhysRevE.89.022114>

[15] D.T. Robb, Y.H. Xu, O. Hellwig, J. McCord, A. Berger, M.A. Novotny, P.A. Rikvold, Evidence for a dynamic phase transition in  $[Co/Pt]_3$  magnetic multilayers. *Phys. Rev. B* **78**, 134422 (2008). <https://doi.org/10.1103/PHYSREVB.78.134422/FIGURES/9/MEDIUM>. URL <https://journals.aps.org/prb/abstract/10.1103/PhysRevB.78.134422>

[16] A. Berger, O. Idigoras, P. Vavassori, Transient behavior of the dynamically ordered phase in uniaxial cobalt films. *Phys. Rev. Lett.* **111**, 190602 (2013). <https://doi.org/10.1103/PHYSREVLETT.111.190602/FIGURES/4/MEDIUM>. URL <https://journals.aps.org/prl/abstract/10.1103/PhysRevLett.111.190602>

[17] P. Riego, P. Vavassori, A. Berger, Metamagnetic anomalies near dynamic phase transitions. *Phys. Rev. Lett.* **118**, 117202 (2017). <https://doi.org/10.1103/PHYSREVLETT.118.117202/FIGURES/5/MEDIUM>. URL <https://journals.aps.org/prl/abstract/10.1103/PhysRevLett.118.117202>

- [18] M. Quintana, A. Berger, Verification of scaling behavior near dynamic phase transitions for nonantisymmetric field sequences. *Phys. Rev. E* **109**, 054112 (2024). URL <https://doi.org/10.1103/PhysRevE.109.054112>
- [19] B. Li, W. Wang, Dynamic magnetic characteristics of the kinetic Ising model under the influence of randomness. *Phys. Rev. E* **110**, 034134 (2024). URL <https://doi.org/10.1103/PhysRevE.110.034134>
- [20] Y. Yüksel, Testing the generalized conjugate field formalism in the kinetic Ising model with nonantisymmetric magnetic fields: A Monte Carlo simulation study. arXiv.org 2411.13119 (2024). URL <https://doi.org/10.48550/arXiv.2411.13119>
- [21] G.M. Buendía, P.A. Rikvold, Fluctuations in a model ferromagnetic film driven by a slowly oscillating field with a constant bias. *Phys. Rev. B* **96**, 134306 (2017). <https://doi.org/10.1103/PHYSREVB.96.134306/FIGURES/7/MEDIUM>. URL <https://journals.aps.org/prb/abstract/10.1103/PhysRevB.96.134306>
- [22] C. Mendes, G.M. Buendía, P.A. Rikvold, Numerical simulation of a two-dimensional Blume-Capel ferromagnet in an oscillating magnetic field with a constant bias. *Phys. Rev. E* **110**, 044133 (2024)
- [23] P.A. Rikvold, H. Tomita, S. Miyashita, S.W. Sides, Metastable lifetimes in a kinetic Ising model: Dependence on field and system size. *Phys. Rev. E* **49**, 5080 (1994). <https://doi.org/10.1103/PhysRevE.49.5080>. URL <https://journals.aps.org/pre/abstract/10.1103/PhysRevE.49.5080>
- [24] K. Binder, P. Virnau, Overview: Understanding nucleation phenomena from simulations of lattice gas models. *J. Chem. Phys.* **145**, 211701 (2016)
- [25] A. Kolmogorov, A statistical theory for the recrystallization of metals. *Bull. Acad. Sci. USSR, Phys. Ser.* **1**, 355–359 (1937)
- [26] W. Johnson, R. Mehl, Reaction kinetics in processes of nucleation and growth. *Trans. Am. Inst. Mining and Metallurgical Engineers* **135**, 416–442 (1939)
- [27] M. Avrami, Kinetics of phase change. *J. Chem. Phys.* **7**, 1103 (1939)
- [28] M. Avrami, *J. Chem. Phys.* **8**, 212 (1940)
- [29] M. Avrami, *J. Chem. Phys.* **9**, 177 (1941)
- [30] R.A. Ramos, P.A. Rikvold, M.A. Novotny, Test of the Kolmogorov-Johnson-Mehl-Avrami picture of metastable decay in a model with microscopic dynamics. *Phys. Rev. B* **59**, 9053–9069 (1999)
- [31] I.D. Lawrie, S. Sarbach, *Phase transitions and critical phenomena*, vol. 9 (Academic Press, 1984)

- [32] J.B. Collins, P.A. Rikvold, E.T. Gawlinski, Finite-size scaling analysis of the  $S = 1$  Ising model on the triangular lattice. *Phys. Rev. B* **38**, 6741–6750 (1988). <https://doi.org/10.1103/PhysRevB.38.6741>. URL <https://link.aps.org/doi/10.1103/PhysRevB.38.6741>
- [33] N.B. Wilding, Coexistence curve singularities at critical end points. *Phys. Rev. Lett.* **78**, 1488–1491 (1997). <https://doi.org/10.1103/PhysRevLett.78.1488>. URL <https://link.aps.org/doi/10.1103/PhysRevLett.78.1488>
- [34] W. Selke, J. Oitmaa, Monte Carlo study of mixed-spin  $S = (1/2, 1)$  Ising ferromagnets. *J. Phys.: Condens. Matter* **22**(7), 076004 (2010). <https://doi.org/10.1088/0953-8984/22/7/076004>. URL <https://dx.doi.org/10.1088/0953-8984/22/7/076004>
- [35] D. Silva, G.M. Buendía, P.A. Rikvold, Multicritical bifurcation and first-order phase transitions in a three-dimensional Blume-Capel antiferromagnet. *Phys. Rev. E* **108**, 024122 (2023). <https://doi.org/10.1103/PhysRevE.108.024122>. URL <https://link.aps.org/doi/10.1103/PhysRevE.108.024122>
- [36] M. Blume, V.J. Emery, R.B. Griffiths, Ising model for the  $\lambda$  transition and phase separation in  $\text{He}^3\text{-He}^4$  mixtures. *Phys. Rev. A* **4**, 1071 (1971). <https://doi.org/10.1103/PhysRevA.4.1071>. URL <https://journals.aps.org/pra/abstract/10.1103/PhysRevA.4.1071>
- [37] J.G. Brankov, J. Przystawa, E. Praveczi, Effect of crystal field anisotropy on the Curie temperature of an Ising ferromagnet: HTS expansion method. *J. Phys. C* **5**(23), 3387 (1972). <https://doi.org/10.1088/0022-3719/5/23/011>. URL <https://dx.doi.org/10.1088/0022-3719/5/23/011>
- [38] T.W. Burkhardt, H.J.F. Knops, Renormalization-group results for the Blume-Capel model in two and three dimensions. *Phys. Rev. B* **15**, 1602–1605 (1977). <https://doi.org/10.1103/PhysRevB.15.1602>. URL <https://link.aps.org/doi/10.1103/PhysRevB.15.1602>
- [39] W.M. Ng, J.H. Barry, Cluster-variation method applied in the pair approximation to the  $S = 1$  Ising ferromagnet having additional single-ion-type uniaxial anisotropy. *Phys. Rev. B* **17**, 3675–3683 (1978). <https://doi.org/10.1103/PhysRevB.17.3675>. URL <https://link.aps.org/doi/10.1103/PhysRevB.17.3675>
- [40] T. Balcerzak, J. Tucker, The spin 1 Blume-Capel model with RKKY interactions. *J. Magn. Magn. Mater.* **278**(1), 87–95 (2004). <https://doi.org/https://doi.org/10.1016/j.jmmm.2003.11.377>. URL <https://www.sciencedirect.com/science/article/pii/S0304885303019735>
- [41] A. Zaim, Y.E. Amraoui, M. Kerouad, H. Arhchoui, Monte Carlo study of the spin-1 Blume-Capel Ising film. *J. Magn. Magn. Mater.* **320**, 1030–1034 (2008). <https://doi.org/10.1016/J.JMMM.2007.10.019>

- [42] W. Kwak, J. Jeong, J. Lee, D.H. Kim, First-order phase transition and tricritical scaling behavior of the Blume-Capel model: A Wang-Landau sampling approach. *Phys. Rev. E* **92**, 022134 (2015). <https://doi.org/10.1103/PHYSREVE.92.022134/FIGURES/8/MEDIUM>. URL <https://journals.aps.org/pre/abstract/10.1103/PhysRevE.92.022134>
- [43] E. Vatansever, N.G. Fytas, Dynamic phase transition of the Blume-Capel model in an oscillating magnetic field. *Phys. Rev. E* **97**, 012122 (2018). <https://doi.org/10.1103/PHYSREVE.97.012122/FIGURES/15/MEDIUM>. URL <https://journals.aps.org/pre/abstract/10.1103/PhysRevE.97.012122>
- [44] A. Malakis, A.N. Berker, I.A. Hadjiagapiou, N.G. Fytas, T. Papakonstantinou, Multicritical points and crossover mediating the strong violation of universality: Wang-Landau determinations in the random-bond  $d = 2$  Blume-Capel model. *Phys. Rev. E* **81**, 041113 (2010). <https://doi.org/10.1103/PHYSREVE.81.041113/FIGURES/11/MEDIUM>. URL <https://journals.aps.org/pre/abstract/10.1103/PhysRevE.81.041113>
- [45] M. Schick, W.H. Shih, Spin-1 model of a microemulsion. *Phys. Rev. B* **34**, 1797 (1986). <https://doi.org/10.1103/PhysRevB.34.1797>. URL <https://journals.aps.org/prb/abstract/10.1103/PhysRevB.34.1797>
- [46] Y. Yüksel, Ümit Akıncı, E. Vatansever, Metamagnetic anomalies in the kinetic Blume-Capel model with arbitrary spin. *Phys. A (Amsterdam, Neth.)* **603**, 127867 (2022). <https://doi.org/10.1016/J.PHYSA.2022.127867>
- [47] P.A. Rikvold, B.M. Gorman, in *Annual Reviews of Computational Physics I*, ed. by D. Stauffer (World Scientific, Singapore, 1994), pp. 149–191
- [48] E.N.M. Cirillo, E. Olivieri, Metastability and nucleation for the Blume-Capel model. Different mechanisms of transition. *J. Stat. Phys.* **83**, 473–554 (1996)
- [49] E.N.M. Cirillo, V. Jacquier, C. Spitoni, Homogeneous and heterogeneous nucleation in the three-state Blume-Capel model. *Physica D – Nonlinear Phenomena* **461**, 134125 (2024). <https://doi.org/10.1016/j.physd.2024.134125>. And references therein
- [50] D. Mataragkas, A. Vasilopoulos, N.G. Fytas, D.H. Kim, Tricriticality and finite-size scaling in the triangular Blume-Capel ferromagnet. *Phys. Rev. Res.* **7**, 013214 (2025). URL <https://doi.org/10.1103/PhysRevResearch.7.013214>

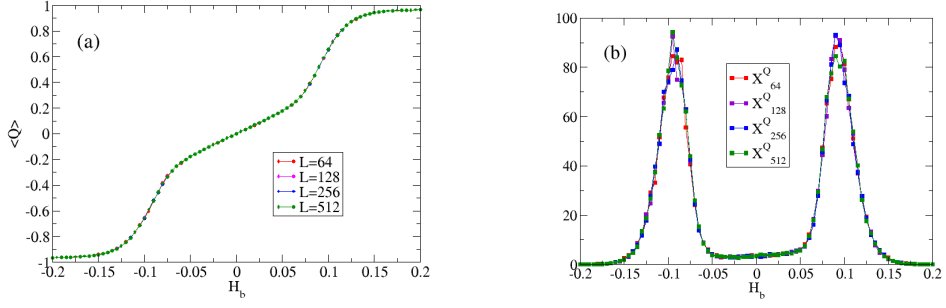


**Fig. 1** Plots of the order parameter  $\langle Q \rangle$  (a), and the scaled variance  $\chi_L^Q$  (b) vs  $H_b$  for the kinetic Ising model.  $P = 1000$  MCSS  $\approx 3.9P_c$ . For this range of sizes, we cannot detect any finite-size effects. Error bars are smaller than the symbol size. See discussion of this figure in Sec. 3. Figures adapted from Ref. [21] with permission.

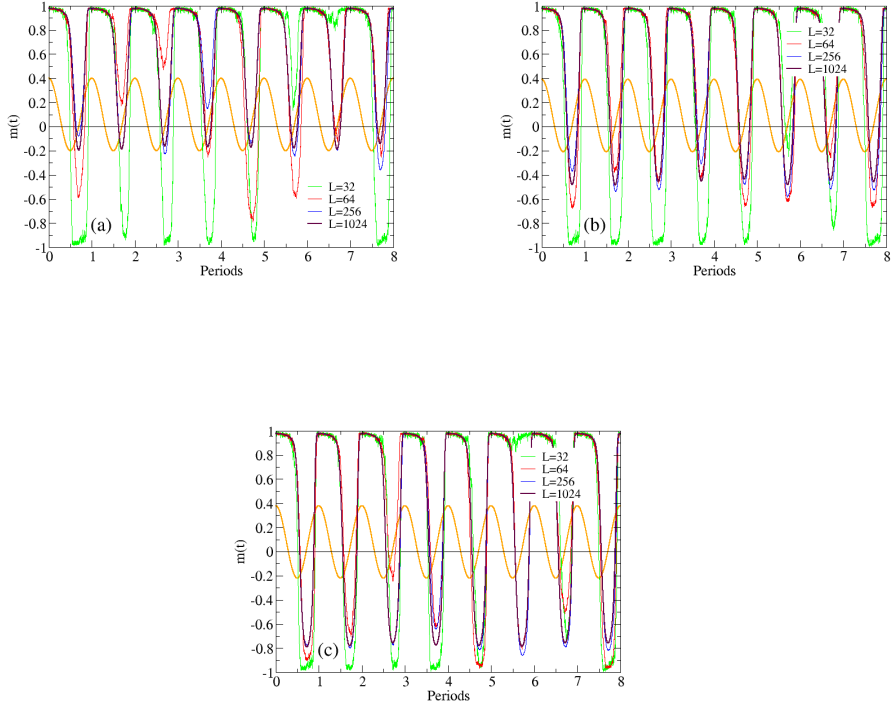


**Fig. 2** Time dependent magnetization  $m(t)$  over eight cycles following a  $200P$  stabilization run for the kinetic Ising model. The orange curves are the total applied field,  $H(t) + H_b$ . The bias is always positive, and  $P = 1000$  MCSS. (a)  $H_b = +0.10$ , just on the strong-bias side of the fluctuation peak (b)  $H_b = H_b^{\text{peak}} = +0.0915$ , at the maximum of the fluctuation peak. (c)  $H_b = +0.08$ , just on the weak-bias side. The switching is stochastic for the smaller systems (SD regime), becoming more deterministic with increasing  $L$  (MD regime). Figures adapted from Ref. [21] with permission.

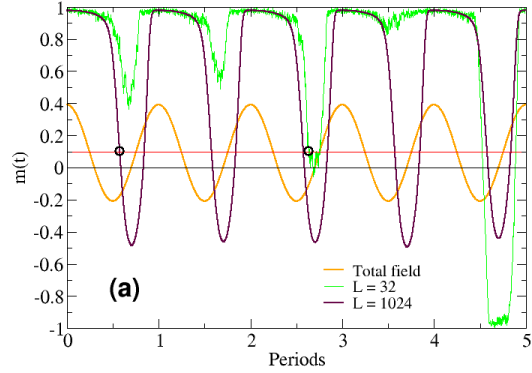


**Fig. 3** A short time series and snapshots showing the growth of disfavored-phase clusters in the kinetic Ising model for  $P = 1000$  MCSS at the corresponding peak position,  $H_b^{\text{peak}} = +0.0915$ . (a) Time series  $m(t)$  over five periods, following  $200P$  stabilization, for  $L = 32$  (green) and  $1024$  (maroon). The total applied field,  $H(t) + H_b$ , is shown in orange. The snapshots were captured the first time that  $m(t)$  fell below  $+0.1$  (red horizontal line), corresponding to a disfavored-phase (down-spin) fraction of 0.45. The times of capture are marked by black circles. In the snapshots, up spins are green, and down spins are red. (b)  $L = 32$ . A single droplet of the down-spin phase has nucleated near the time when the total applied field has its largest negative value. The stochastic nature of the SD switching mode is also evident in part (a). (c)  $L = 1024$ . Many down-spin droplets have nucleated at different times and then grown almost independently. At the moment of capture, some clusters have coalesced while others are still growing independently. From part (a) it is seen that this MD switching mode leads to a nearly deterministic evolution of  $m(t)$ . Figures adapted from Ref. [21] with permission.

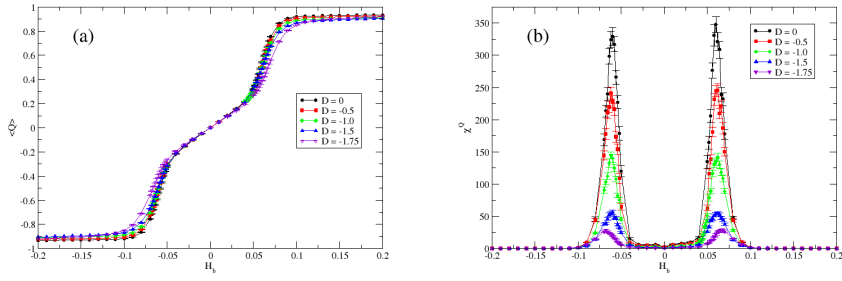


**Fig. 4** Dependence of the sidebands for the kinetic BC model on the crystal field  $D$  for  $L = 128$ . Here,  $D \in [-1.75, 0]$ , so zeros are significant. For each value of  $D$ , we maintained  $P \approx 4P_c(D)$  and  $T = 0.8T_c(D)$ . The values of  $P_c(D)$ ,  $|H_b^{\text{peak}}|$ , and  $T_c(D)$  are given in Table 1. (a)  $\langle Q \rangle$  vs  $H_b$ . (b)  $\chi^Q$ . The peak heights decrease with increasing  $D$ , while  $|H_b^{\text{peak}}|$  increases slightly as  $D$  approaches  $D_t$ . Figures from Ref. [22] under CC-BY 4.0 license.

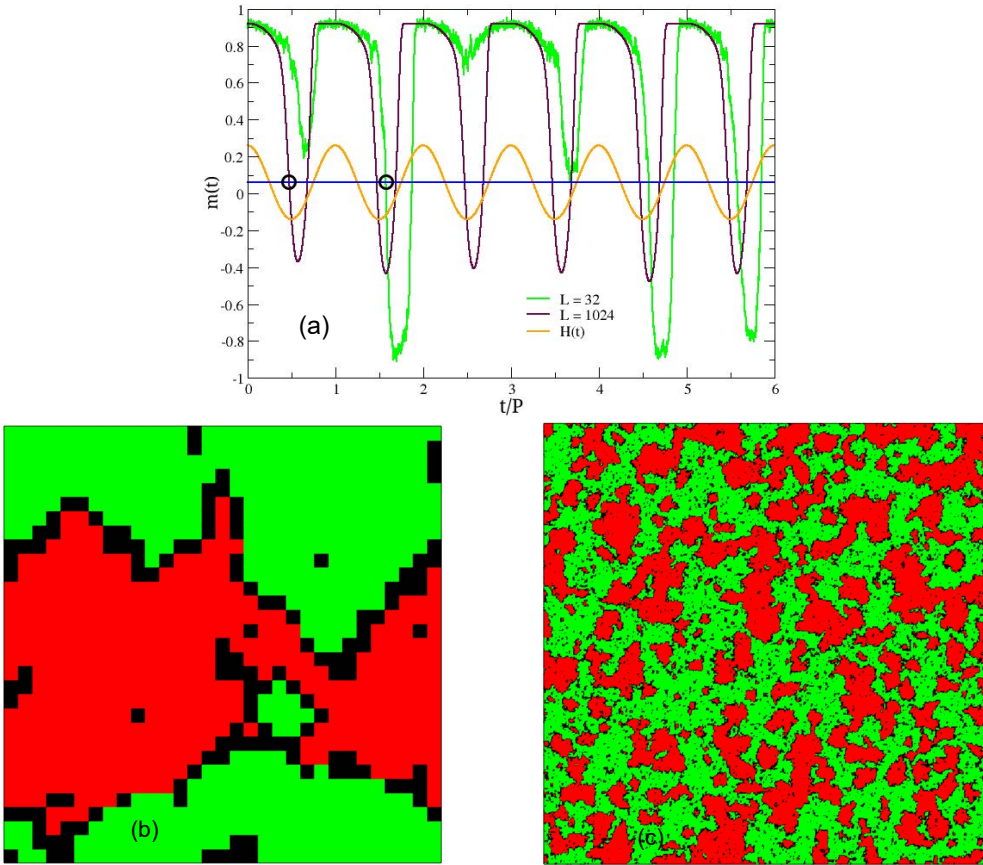


**Fig. 5** Results for the kinetic BC model. (a)  $m(t)$  over six periods for  $L = 32$  and  $L = 1024$ . The total applied field  $H(t) + H_b$ , with  $D = -1.5$ ,  $P = 820 \approx 4P_c$  and  $H_b = 0.063 \approx |H_b^{\text{peak}}|$ , is shown in orange. Snapshots of the lattice were taken for both sizes when  $m(t)$  first reached the threshold of 0.063 (blue horizontal line). The times of capture are marked by black circles. For this threshold value,  $H(t) + H_b < 0$ , so the disfavored configuration of down-spins is the stable state, which is shown in red. Up-spins are shown in green, and zeros in black. (b) Snapshot for  $L = 32$ . The decay occurs by the SD mechanism. (c) Snapshot for  $L = 1024$ . The decay occurs by the MD mechanism. In both snapshots, the zeros accumulate at the cluster boundaries. Figures reproduced from Ref. [22] under CC-BY 4.0 license.

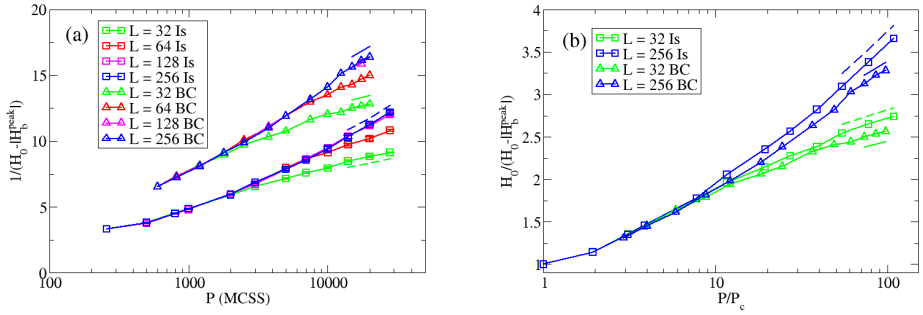


**Fig. 6** Linear vs logarithmic plots of peak positions vs oscillation period, corresponding to the nucleation-theoretical relation, Eq. (7). (a) Data for the Ising model [21] and the BC model [22], displayed together. As the simulations were performed with different values of  $H_0$ , 0.3 and 0.2, respectively, the results do not coincide. (b) The same data, plotted in terms of the dimensionless variables,  $1/(1 - H_b^{\text{peak}}/H_0)$  and  $P/P_c(H_0)$ . The scaled data coincide for  $P/P_c < 10$ . For  $P/P_c > 10$ , results for the different models and different system sizes separate, as predicted by the theory. See further discussion in Sec. 5. Data obtained from Refs. [21] with permission and from [22] under CC-BY 4.0 license.